THE JOURNAL OF PHYSICAL CHEMISTRY Letters

Letter

pubs.acs.org/JPCL

Optimization of Spectral and Spatial Conditions to Improve Super-Resolution Imaging of Plasmonic Nanoparticles

A. Swarnapali De Silva Indrasekara,[†,#] Bo Shuang,[†] Franziska Hollenhorst,[†] Benjamin S. Hoener,[†] Anneli Hoggard,[†] Sishan Chen,[†] Eduardo Villarreal,[‡] Yi-Yu Cai,[†] Lydia Kisley,[†,⊥] Paul J. Derry,[†] Wei-Shun Chang,[†] Eugene R. Zubarev,[†,‡] Emilie Ringe,[†,‡] Stephan Link,[*,†,§] and Christy F. Landes[*,†,§]

[†]Department of Chemistry, Rice University, 6100 Main Street, MS-60, Houston, Texas 77005, United States

[‡]Department of Materials Science and Nanoengineering, Rice University, 6100 Main Street, MS-325, Houston, Texas 77005, United States

[§]Department of Electrical and Computer Engineering, Rice University, 6100 Main Street, MS-366, Houston, Texas 77005, United States

Supporting Information

ABSTRACT: Interactions between fluorophores and plasmonic nanoparticles modify the fluorescence intensity, shape, and position of the observed emission pattern, thus inhibiting efforts to optically super-resolve plasmonic nanoparticles. Herein, we investigate the accuracy of localizing dye fluorescence as a function of the spectral and spatial separations between fluorophores (Alexa 647) and gold nanorods (NRs). The distance at which Alexa 647 interacts with NRs is varied by layer-by-layer polyelectrolyte deposition while the spectral separation is tuned by using NRs with varying localized surface plasmon resonance (LSPR) maxima. For resonantly coupled Alexa 647 and NRs, emission to the far field through the NR plasmon is highly prominent, resulting in underestimation of NR sizes. However, we demonstrate that it is possible to improve the accuracy of the emission localization when both the spectral and spatial separations between Alexa 647 and the LSPR are optimized.

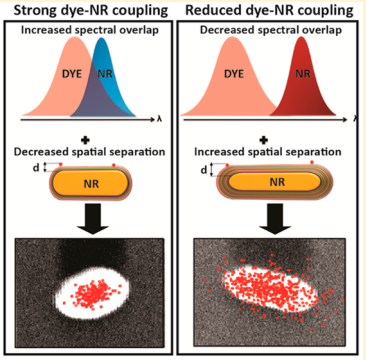

Super-resolution microscopy has been employed to study dynamic interactions at the surface of plasmonic nanomaterials,[1] to visualize the electromagnetic field distribution around nanomaterials,[2] to investigate nanoparticle surface chemistry,[3−6] and to explore the potential for in situ imaging.[2,7−11] Coupling of the fluorophore emission with plasmonic nanomaterials was shown to alter the photophysics of the fluorophore and to affect its emission localization, thereby diminishing the accuracy of mapping the size and shape of plasmonic nanoparticles by super-resolution imaging techniques.[6,10,12−16]

Resonant coupling between fluorophore emission and the localized surface plasmon resonance (LSPR) of nanoparticles can enhance the collected fluorescence intensity.[17−21] Larger photon count rates lead to an increase in the precision of localization imaging,[22] but coupling of dyes to metal nanoparticles has recently been reported to negatively affect the accuracy of super-resolution mapping.[23] It has been proposed that the emission of fluorophores in close proximity to plasmonic nanoparticles can occur by two competing radiative pathways: directly into the far field or through the LSPR of the nanoparticles.[10,24−27] The latter results in a displacement of the single molecule emission centroids toward the center of the plasmonic nanoparticle, leading to an underestimation of nanoparticle size and shape by super-resolution microscopy.[10,12,12,23,28,29] Experimental optimizations such as tuning the density of fluorophores on the surface of gold nanorods (NRs), adjusting the spatial separation between fluorophores and NRs, and changing the identity of the fluorophores can reduce the nanoparticle−dye coupling.[28] However, none of these approaches have been able to generate super-resolution images of plasmonic nanoparticles that match well with their true dimensions. Another complication is that the point spread function (PSF) of the fluorophore emission near plasmonic nanoparticles is distorted, leading to an inaccurate determination of the true emission location, for which no solution has yet been found.[12−14]

Two possible processes have been identified to affect the accuracy of super-resolution imaging of plasmonic nanomaterials: the spatial separation between the fluorophores and the nanoparticle and the spectral overlap between the fluorophore emission and the LSPR maximum that governs the strength of the dipole−optical antenna coupling.[10,23,28] These key parameters have been investigated using various super-resolution techniques[5,8,13,15,23] and for different chemical and molecular interactions between plasmonic nanoparticles and fluorophores.[10,13,15,28] What is still missing and desperately needed to advance this field is an examination of the interplay

Received: November 3, 2016
Accepted: December 16, 2016
Published: December 16, 2016

DOI: 10.1021/acs.jpclett.6b02569
J. Phys. Chem. Lett. 2017, 8, 299−306

between these two parameters and particularly their impact on the accurate mapping of plasmonic materials.

Here, we investigated the accuracy of the size and shape obtained for gold NRs using super-resolution imaging as a function of the fluorophore−NR coupling strength, as tuned via both spatial and spectral separations between the fluorophores and the NRs. Stochastic electrostatic interactions of negatively charged Alexa 647 fluorophores with positively charged layer-by-layer polyelectrolyte (PE)-coated NRs were exploited to reconstruct super-resolution images of NRs by motion-blur point accumulation for imaging in nanoscale topography (mbPAINT).[30] The spatial separation was tuned by changing the number of PE layers around the NRs[15,31−33] while the spectral overlap was varied using NRs with different LSPR maxima compared to the emission spectrum of Alexa 647. Correlated scanning electron microscopy (SEM) was used to confirm the accuracy of the NR sizes obtained from mbPAINT. We found that the optimization of both the spectral and spatial separations between fluorophores and NRs is critical to obtain the correct emission positions and hence improved accuracy in super-resolution imaging of plasmonic nanostructures. When there is a greater spectral overlap, even a larger spatial separation results in sufficient coupling between the fluorophore emission and the NR, to alter the far-field emission location. On the other hand, for nonresonantly coupled fluorophore−NR systems, direct far-field emission is facilitated only when the coupling between the fluorescence and the NR LSPR is reduced by a sufficiently large spatial separation controlled by the number of PE layers around the NR.

The distance between Alexa 647 molecules and single NRs was varied via layer-by-layer PE deposition (Figure 1).[32,33] Alternating layers of poly(3,4-ethylenedioxythiophene)-polystyrenesulfonate (PSS) and polydiallyldimethylammonium chloride (PDADMAC) were deposited on cetyltrimethylammonium bromide (CTAB)-coated NRs in sequence until the desired number of PE layers with a terminating positive charge was obtained (Figure 1a; see the Supporting Information (SI); Experimental Section). Ensemble UV−visible spectra showed no significant change in the LSPR maxima of NRs upon PE deposition (Figure 1b), indicating the colloidal stability of PE-coated NRs in water. In the representative UV−visible spectra shown in Figure 1b, the LSPR maxima for both CTAB NRs and the PE-coated NRs are at 732 nm. Successful layer-by-layer PE coating of NRs was also evident by zeta potential measurements (Figure S1). Transmission electron microscopy (TEM) analysis confirmed the presence of PE layers on the NRs (Figures 1c and S2).[32,33] High-resolution TEM (HRTEM) image analysis showed that the thickness of the PE spacer on the NRs is nonuniform (Figure S3). The mean of the average spacer thickness of NRs coated with 2, 4, and 6 PE layers in their dry state, as determined by HRTEM, was 1.3 ± 0.3, 1.4 ± 0.3, and 3.1 ± 0.8 nm, respectively (Figure S3). However, as reported in the literature, due to the well-known phenomenon of polymer swelling in solution,[34−37] the thickness of the hydrated PE spacer on NRs during mbPAINT is predicted to be much larger than that obtained from HRTEM. Despite local variations of spacer layer thickness around individual nanostructures (Figure S2), the PE coating satisfied our need for a tunable spacer layer with a high packing density for mbPAINT experiments (see also Figure S4). For the work reported here, we used NRs with varying aspect ratios (Figure S5) and LSPR maxima between 650 and 850 nm and coated them with varying PE layers, thereby varying spacer thickness.[15,32,33]

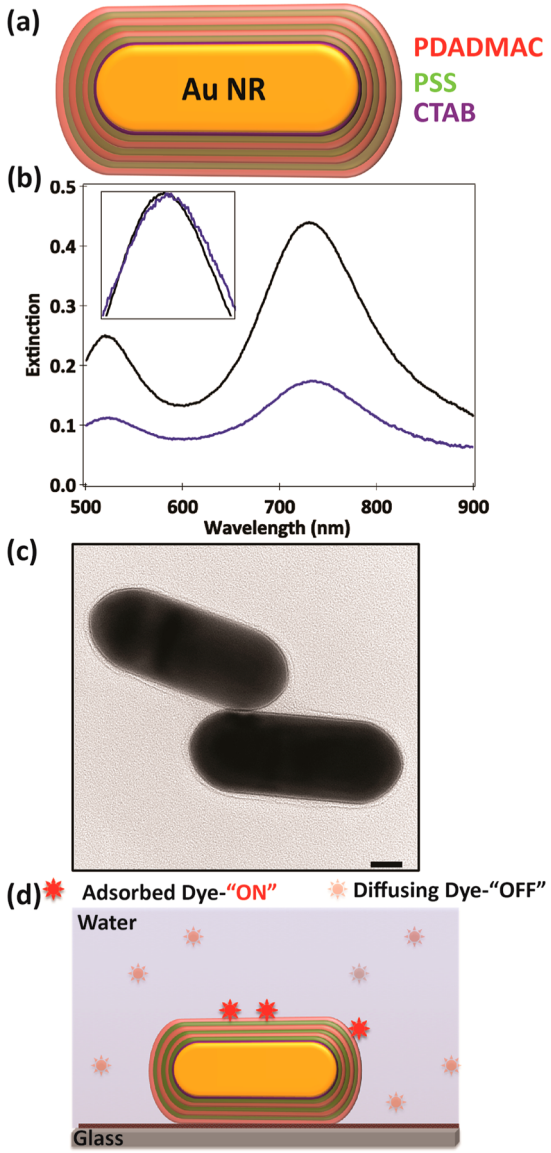

Figure 1. (a) Schematic representation of a layer-by-layer PE-coated NR. Purple, CTAB bilayer; green, PSS; pink, PDADMAC. (b) Representative ensemble UV−visible spectra of CTAB-capped NRs before (black) and after (blue) PE coating in water. The decrease in extinction for the PE-coated NRs resulted from a decrease in the NR concentration following the layer-by-layer PE coating and the purification steps. (Inset) Normalized extinction spectra of the NRs before and after PE coating, indicating that the change in the LSPR maximum is negligible after PE coating. The LSPR maximum is at 732 nm. (c) Representative TEM micrograph of NRs coated with six layers of PE. The light colored layer around the NRs shows the presence of the PE layer around the NRs having average dimensions of 44 nm × 121 nm (scale bar, 20 nm). (d) Schematic illustration of the sample geometry used for the super-resolution imaging of NRs with Alexa 647 using mbPAINT. PE-coated NRs immobilized on bovine serum albumin passivated (brown layer) glass coverslips were immersed in an aqueous solution of Alexa 647. Emission from each single Alexa 647 molecule adsorbed onto a NR ("on") was detected by an EMCCD camera, while diffusing/desorbed molecules appear blurred ("off") due to their diffusion being faster than the acquisition rate of the detector.

As depicted in Figure 1d, individual PE-coated NRs immobilized on a glass substrate interacted with single Alexa

DOI: 10.1021/acs.jpclett.6b02569
J. Phys. Chem. Lett. 2017, 8, 299−306

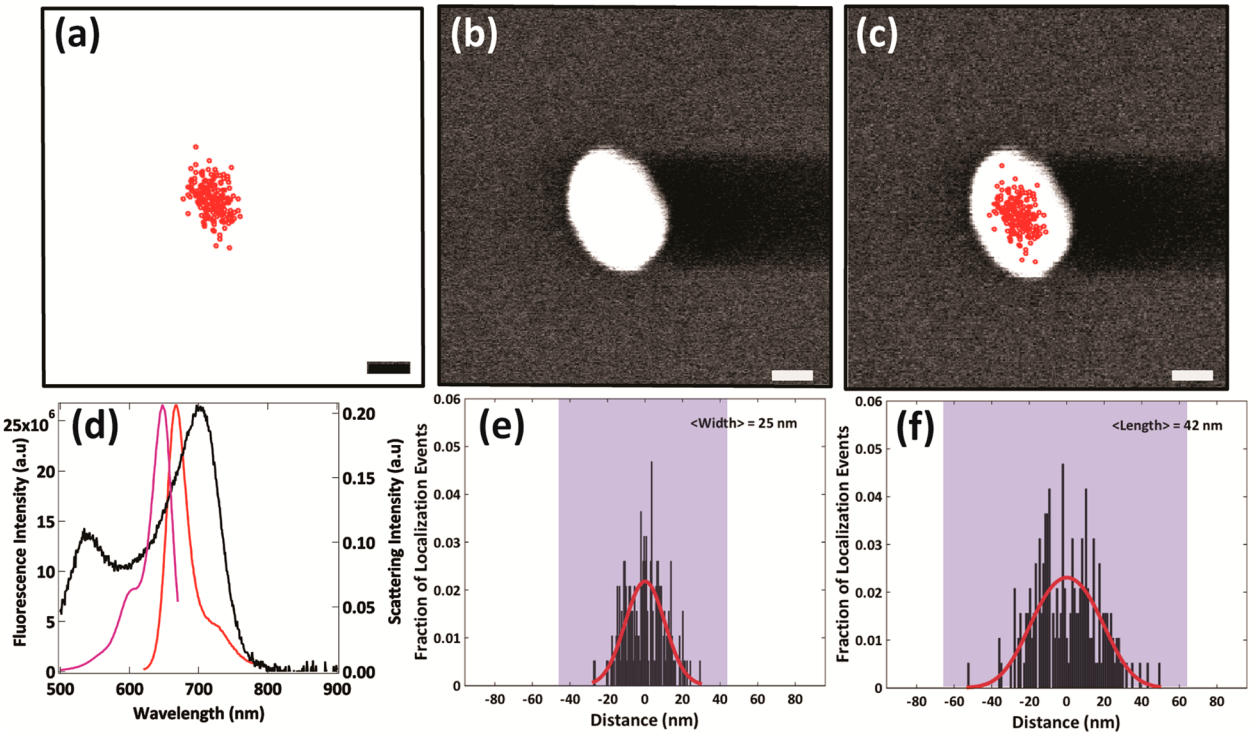

Figure 2. Size of a NR coated with six PE layers is underestimated when there is a significant spectral overlap of the LSPR with the Alexa 647 emission. (a) Super-resolution image showing the positions of all of the emission events over 1000 frames of data collection. Each red marker denotes the position of emission from a single Alexa 647 binding event on the 650NR, (b) corresponding SEM micrograph, and (c) both overlapped for comparison. The scale bar (50 nm) is the same in all images. (d) Single-particle scattering spectrum of the NR coated with six layers of PE in water (black) compared to ensemble fluorescence excitation (pink) and emission (red) spectra of Alexa 647 in phosphate buffered saline. The broad line width of the LSPR is due to the small aspect ratio (1.4) of the NR.[40] (e,f) Histograms of the distribution of localization events across and along the NR displayed in (a) along the width and length of the NR, respectively. The distance of all of the localization events to the center was fitted to the convoluted distribution shown by the red curve. The fwhm of the fitted distribution is used as an estimate of the width and length. The shaded areas show the actual width and length of the NR as determined from SEM. The actual size of the NR from the SEM micrograph is 87 nm × 127 nm, while the dimension of the NR from mbPAINT is 25 nm × 42 nm.

647 molecules in a stochastic manner, which is the underlying principle of mbPAINT (see the SI, Experimental Section).[30] When a negatively charged Alexa 647 molecule electrostatically adsorbed onto the positively charged PDADMAC outer layer of a NR, a strong fluorescence signal was detected, which is referred to as an "on" event. Fluorescence from freely diffusing Alexa 647 molecules was undetectable due to motion-blur and only contributed to background signal.[30] Diffusing/desorbed/photobleached molecules are considered to be in an "off" state. The experiments were carried out under low concentrations of Alexa 647 (2−5 nM) in order to ensure both accurate identification of single molecule "on" events on NRs and a low background. Single binding events were identified based on a local background threshold and local maximum signal intensity (see the SI, Experimental Section).[30,38] Identified adsorption events were then fit to radial symmetry to extract the centroid and static localization uncertainties.[39] The coordinates of all of the centroids over the entire data acquisition period were combined to generate a super-resolved image. The localization analysis resulted in a localization precision of ∼10 nm, thus ensuring that the width and length of NRs determined from mbPAINT were not limited by the spatial resolution of mbPAINT.

When there was significant spectral overlap between the emission of Alexa 647 and the NR LSPR, the sizes of the NRs were underestimated by mbPAINT (Figure 2). This result confirmed earlier reports that emission from fluorophores located in close proximity to plasmonic nanoparticles cannot be accurately localized.[8,12,23] In particular, the sizes of NRs with a LSPR maximum of ≤650 nm and hence a good spectral overlap with the Alexa 647 absorption and emission spectra (Figure 2d) were significantly underestimated (Figure 2a−c). The noticeable broadening of the LSPR was due to the small NR aspect ratio (1.4).[40] This NR was coated with six layers of PE, thereby creating a spatial separation of, on average, ∼4−8 nm[15,32,33] between Alexa 647 and the NR. This spacing was large enough to avoid fluorescence quenching.[20,41] Nevertheless, a comparison between correlated SEM and mbPAINT analysis of this NR revealed the underestimation of both the NR size and shape. Each red marker in Figure 2a represents the emission centroid of a single molecule in a single frame collected over 1000 frames total. The same NR was located in a SEM (Figure 2b) with the aid of an indexed grid on the glass coverslip and imaged for comparison. When the corresponding SEM image of the NR was overlaid with the super-resolution image (Figure 2c), the emission events were highly localized at the center of the NR, demonstrating an inaccurate representation of the NR dimensions by mbPAINT. The actual size of the NR from the SEM image was 87 nm × 127 nm, while the dimension of the NR determined from mbPAINT was 25 nm × 42 nm (Figure 2e,f). Therefore, we conclude that when there is strong spectral overlap, decreasing the spatial overlap is not sufficient to decouple the Alexa 647 emission from the NR LSPR, and the

DOI: 10.1021/acs.jpclett.6b02569
J. Phys. Chem. Lett. 2017, 8, 299−306

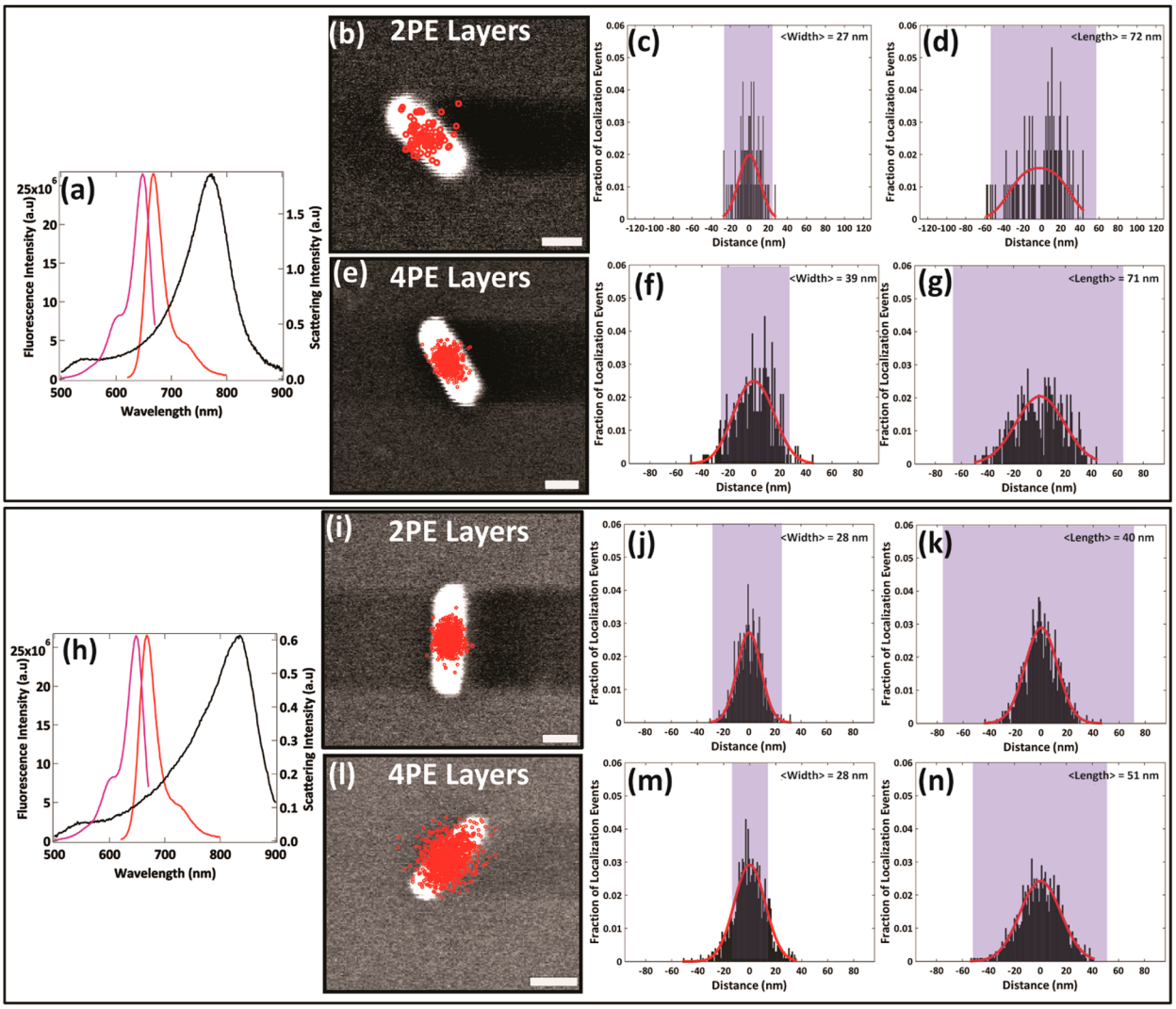

Figure 3. Even with reduced spectral overlap, spatial separation also controls super-resolution accuracy. (a,h) Reduced overlap between the excitation (pink) and emission (red) spectra of Alexa 647 and the single-particle scattering spectra (black) of the representative PE-coated NRs with ensemble LSPR maxima of 770 and 835 nm, respectively. The spectral asymmetry of the latter is at least partly attributed to the limitation of the spectral window of the CCD camera. (b,e) Composite SEM−super-resolution images of NRs coated with (b) two layers (size from SEM 48 nm × 111 nm, size from mbPAINT 27 nm × 72 nm) and (e) four layers of PE (size from SEM 50 nm × 125 nm, size from mbPAINT 39 nm × 71 nm). (i,l) Composite SEM−super-resolution images of NRs coated with (i) two layers (size from SEM 44 nm × 154 nm, size from mbPAINT 28 nm × 40 nm) and (l) four layers of PE (size from SEM 27 nm × 103 nm, size from mbPAINT 28 nm × 51 nm). The scale bar (50 nm) is the same in all images. (c and d, f and g, j and k, m and j) Histograms of the distribution of localization events across and along the NR displayed in (b,e,i,l) along the width and length of the NR, respectively. The areas shaded in blue show the actual width and length of NRs as determined from SEM.

LSPR acting as a dipole antenna determines the far-field emission properties.[12,23,28]

Spectral overlap and spatial separation are both important parameters for super-resolution optical imaging of NRs (Figure 3). NR samples with two different LSPR maxima and two different PE layer thicknesses were imaged with mbPAINT and compared with correlated SEM analysis. Figure 3a,h shows the spectral overlap between the Alexa 647 emission spectrum and single-particle scattering spectra of representative PE-coated NRs with LSPR maxima of 770 and 835 nm, respectively. Each NR sample was coated with two and four PE layers and imaged with mbPAINT (Figure 3b,e,i,l). Even when the LSPR was detuned from the dye emission, mbPAINT underestimated the NR size and shape when compared with correlated SEM images, as shown in Figure 3b,i for the two PE layer system. A spacer of two PE layers is expected to result in a < 5 nm separation between the Alexa 647 molecules and the NRs.[32,33] At this distance, the fluorophore emission is typically quenched by plasmonic nanoparticles.[20,41−43] Ineffective mbPAINT imaging in this case could therefore be due to fluorescence quenching, which reduces the localization precision.[22] In order to evaluate the relative contribution of spacer thickness on the accuracy of mbPAINT imaging, NRs with different PE layers were studied. As shown in Figure 3e,l, mbPAINT still resulted in underestimated NR sizes, even with NRs coated with four layers of PE. Though we observed a variation in the emission intensity as a function of spacer thickness (Figure S6) consistent with quenching for smaller separations, no significant improvement in the accuracy of emission localization was observed with four PE layers as compared to two PE layers. However, unlike in the resonantly coupled conditions depicted in Figure 2, the recovered mbPAINT NR widths for nonresonantly coupled conditions (Figure 3) were comparable to those depicted in SEM, whereas the lengths were still highly

DOI: 10.1021/acs.jpclett.6b02569
J. Phys. Chem. Lett. 2017, 8, 299−306

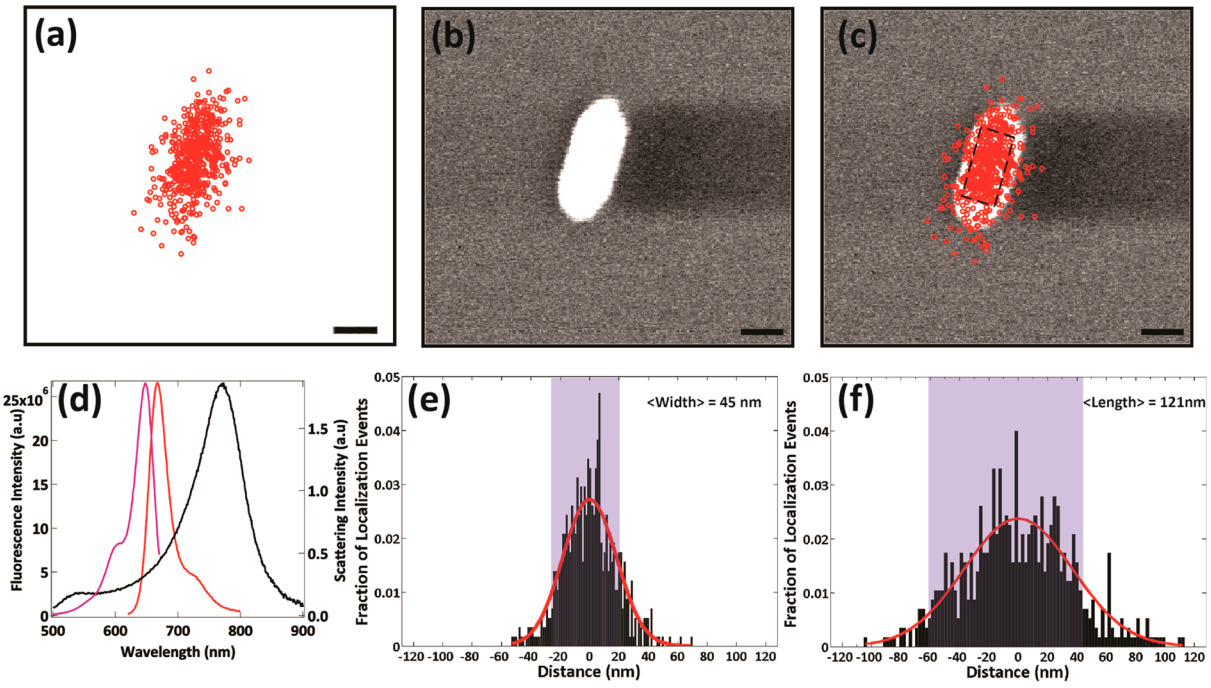

Figure 4. Optimizing both spectral and spatial separations yields improved optical super-resolution imaging. (a) Super-resolution image, (b) corresponding SEM image, and (c) overlapped super-resolution and SEM images for a NR with a LSPR maximum at 785 nm and coated with six layers of PE (scale bars, 50 nm). Dashed lines (black) in (c) show the boundaries for the longitudinal and transverse axes determined by considering the localization events in each direction. These boundaries were later used to calculate the width and length of the super-resolution image of the NR. (d) Reduced overlap between the single-particle scattering spectrum of the NR and the ensemble fluorescence excitation (pink) and emission (red) spectra of Alexa 647. (e,f) Histograms of the distribution of localization events across and along the NR displayed in (a), indicating the width and length of the NR, respectively. The distance of all of the localization events to the center was fitted to the convoluted distribution shown by the red curve. The fwhm of the fitted distribution is used as an estimate of the width and length. The areas shaded in blue show the actual width and length of the NR as determined from SEM. The dimension of the NR from mbPAINT is 45 nm × 121 nm, which agrees well with the actual size of the NR (50 nm × 128 nm) as determined from SEM.

underestimated. The full width at half-maxima (fwhm) of NR widths (27−41 nm) determined by the cross-sectional profiles across the reconstructed super-resolution images (Figure S7) showed fairly good agreement with the actual widths of the NRs as obtained from SEM micrographs (27−50 nm). These results show that spectral detuning is one contributor for better super-resolution imaging but alone is not sufficient to yield accurate sizes.

Improved NR sizes and shapes are extracted only if both the spectral and spatial separations between the Alexa 647 molecules and NRs are optimized. Figure 4 compares SEM and mbPAINT analysis of a NR with six layers of PE and a LSPR maximum at 785 nm, which satisfied both spatial and spectral separation requirements. The 2D Gaussian distribution of all of the localization events along the transverse and longitudinal axes of the localization image was convoluted with a rectangular uniform distribution. Here, we assumed that the emission localization is uniform over the NR and that the shape of the NR can be approximated as a rectangle. The fwhm of the fitted distribution, which represents the distribution of all localization events, was then used as an estimate of the width and length of the NR (see details in the SI and Figure 4e,f). The calculated dimensions from mbPAINT (45 nm × 121 nm) showed very good agreement with those measured by SEM (50 nm × 128 nm). A summary of the relationship between the dye−NR spectral and spatial separations and the dimensions determined from mbPAINT are provided in Figure 5. This analysis indicated that improved localization accuracy can be achieved only when the LSPR maxima of the NRs is minimally

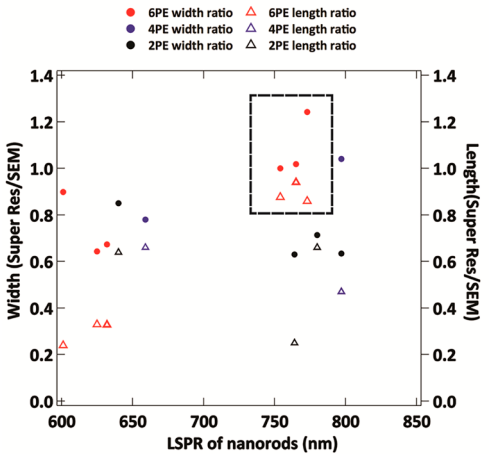

Figure 5. Correlation of the spectral overlap between Alexa 647 and the NR LSPR as well as PE spacer thickness with the improved size determination from super-resolution imaging of NRs. The width and length from mbPAINT are normalized to the values obtained from SEM and given as a ratio. The LSPR maxima for the NRs shown here are determined either by correlated single-particle dark-field scattering spectroscopy or Gans theory. The area marked in dotted lines indicates the optimum spacer thickness and NR LSPR maxima for the NRs studied here using mbPAINT with Alexa 647.

overlapped with the Alexa 647 emission (at least LSPR ≥ 750 nm) and when the NRs have a thick spacer (at least six PE layers). Qualitative analysis of TEM micrographs (Figure S3)

DOI: 10.1021/acs.jpclett.6b02569
J. Phys. Chem. Lett. 2017, 8, 299−306

showed that the thickness of the PE layer on the NRs was not uniform; it varied among different NRs but also for the same NR, resulting in some NRs having a thinner PE spacer layer than expected. This means that even for some NRs with six layers of PE, the super-resolution images underestimated the size and shape. This limitation arises from the solution-based PE functionalization of the NRs, but with optimized preparation of the spacer thickness, we expect a higher success rate for accurate super-resolution imaging of plasmonic nanoparticles.

Our experimental results demonstrate the effects of the dye−NR spatial and spectral separations on the accurate localization of emission events on NRs, which in turn determine the accuracy of super-resolution imaging of NRs. Regardless of the spatial separation, highly prominent reradiation of the fluorescence through the NR was observed in resonantly coupled Alexa 647−NR systems (Figure 2), leading to erroneous super-resolution images. The observed displacements of emission positions can be attributed to strong coupling between Alexa 647 molecules and the NR that acts as a dipole antenna.[10,23,28] Though dipole emitter−optical antenna coupling and its consequences have been discussed,[16,19,20,24,25,27,41−44] a complete mechanistic understanding of the plasmon-controlled dye emission position as necessary for super-resolution imaging has not yet been fully established. In general, fluorophores emitting in close proximity to nanoparticles induce a "mirror" dipole in the nanoparticle.[45] Radiation by the "mirror" dipole to the far field therefore makes it seem as if the nanoparticle is the emitting species.[27] Recording these modified emission positions results in the observed localization events being co-localized with the NR center, thereby leading to inaccurate reconstructed super-resolution images (Figure 2). When the Alexa 647−NR system was spectrally detuned, we observed two different outcomes. (1) When the spatial separation between the Alexa 647 molecules and the NR was small, the centroids of the emission events still appeared to accumulate at the NR center (Figure 3), consistent with previous work.[10] However, with four PE layer coatings (Figure 3e,l), the estimation of the widths of NRs by mbPAINT was improved but not the lengths. This could be related to the highest local E-field enhancement that exists at the tips of NRs,[42] which requires larger spatial separation between the dye and the NR. We assume that this could also be the reason for the stronger distortion of the apparent emission position along the length of NRs. (2) When the spatial separation between the Alexa 647 molecules and the NR was increased by employing six PE layer coatings, a distribution of emission events over a larger area of the NR, away from the center, was observed. Given that the thickness of the hydrated PE is much larger than their dry state (3.1 ± 0.8 nm, Figure S3),[34−37] the spacer of NRs with six PE layers is expected to exceed 5 nm. On the basis of our results, as both spatial and spectral separations reach an optimum, fluorophore−NR coupling becomes much weaker, and thus, the generation of and radiation from "mirror" dipoles is less prominent. Therefore, both the emission and the associated apparent location most likely represent the far-field emission from the fluorophore and its true position on the NR, respectively. This result differs from earlier work that found coupling between fluorophores and plasmonic nanoparticles even for non-resonantly coupled systems at separations as large as 90 nm.[10] However, given the relatively narrower LSPR peaks of our NRs, the spectral overlap is smaller here, which should result in weaker fluorophore−NR coupling, thereby allowing us to resolve the emission positions accurately (Figure 4).

Although we have demonstrated methods to improve the super-resolution imaging of plasmonic nanoparticles through optimized experimental conditions, several additional challenges must be overcome to achieve consistent accuracy. Heterogeneity in the PE layer thickness can be overcome by optimizing the fabrication protocol. Another challenge is the estimation of the PE layer thickness for individual NRs as the PE layer cannot be visualized by SEM imaging due to the inherent radiation sensitivity of polymers. The incorporation of negative staining practices for SEM imaging[46] should make it easier to visualize and collect PE spacer thickness information for single NRs. Thus, the combination of these two improvements will allow us to determine the effective PE spacer thickness in its hydrated state during mbPAINT and correlate it to the thickness in its dry state from SEM. One additional issue is the increasing surface desorption of the coated NRs. Over the course of the correlated measurements, which include wide-field, SEM, and dark-field spectroscopy, desorption of NRs occurs, which for every sample decreases the available sample size for analysis. Stronger immobilization chemistry would improve sample retention.

In conclusion, we demonstrated the synergy between the spatial and spectral separations of fluorophores and NR LSPRs for accurate size and shape determination by mbPAINT. Stochastic adsorption and desorption/photobleaching of Alexa 647 on NRs with varying PE spacer thicknesses and LSPR maxima were used to construct super-resolution images of NRs. In a nonresonantly interacting fluorophore−NR system with sufficient spatial separation between fluorophores and NRs, the coupling between the fluorophore emission and LSPR is strongly reduced. This decoupling allows the molecular fluorescence to be radiated into the far field directly instead of through the NR LSPR and in turn allows the emission events to appear at their true locations. With optimized experimental conditions, mbPAINT can be employed to map the NR shapes and sizes that agree very well with the true dimensions. Given the heterogeneity in PE layer thickness around individual NRs and the further variation from particle to particle, further optimization is still required to achieve accurate size and shape determination for all NRs within a sample. Our findings provide an important step toward solving the important issue that the super-resolution imaging community has been dealing with for plasmonic nanoparticles; the inability to reconstruct super-resolved images that match the actual nanoparticle morphology.

■ ASSOCIATED CONTENT

Supporting Information

The Supporting Information is available free of charge on the ACS Publications website at DOI: 10.1021/acs.jpclett.6b02569.

Detailed procedures for NR functionalization and characterization, super-resolution imaging experiments and data analysis, and super-resolution imaging of gold nanowires with different surface chemistries (PDF)

■ AUTHOR INFORMATION

Corresponding Authors

*E-mail: slink@rice.edu. Phone: 713-348-4561 (S.L.).
*E-mail: cflandes@rice.edu. Phone: 713-348-4232 (C.F.L.).

ORCID

Christy F. Landes: 0000-0003-4163-6497

DOI: 10.1021/acs.jpclett.6b02569
J. Phys. Chem. Lett. 2017, 8, 299−306

Present Addresses

[#]A.S.D.S.I.: Department of Biomedical Engineering, Duke University, Durham, North Carolina 27708, U.S.A.

[⊥]L.K.: University of Illinois at Urbana−Champaign, Beckman Institute, 600 S. Mathews Ave., MC-712, Box C-3, Urbana, Illinois 61801, U.S.A.

Author Contributions

A.S.D.S.I., L.K., W.-S.C., S.L., and C.F.L. designed research and A.S.D.S.I., and F.H. conducted the super-resolution experiments and data analysis; B.S developed the super-resolution data analysis programs; B.S.H. and A.H. conducted the SEM imaging and analysis, Y.-Y.C. and E.V. conducted TEM/HRTEM imaging supervised by E.R.; S.C. conducted DLS and ensemble fluorescence measurements; P.J.D. performed the synthesis and functionalization of nanowires supervised by E.R.Z. A.S.D.S.I., F.H., S.L., and C.F.L. wrote the paper.

Notes

The authors declare no competing financial interest.

■ ACKNOWLEDGMENTS

The authors acknowledge funding from the National Science Foundation (Grant CHE-1151647 to C.F.L.; Grant CBET-1438634 to S.L. and C.F.L.; Grant DMR-1105878 to E.R.Z.), the Welch Foundation (Grants C-1787 to C.F.L. and C-1664 to S.L.), the Air Force Office of Scientific Research (MURI FA9550-15-1-0022 to S.L.), and the American Chemical Society Petroleum Research Fund (54684-ND5 to C.F.L. and 56256-DN15 to E.R.). A.H., L.K., and E.V. acknowledge the National Science Foundation Graduate Research Fellowship (Grant 0940902).

■ REFERENCES

(1) Dominguez-Medina, S.; Kisley, L.; Tauzin, L. J.; Hoggard, A.; Shuang, B.; D. S. Indrasekara, A. S.; Chen, S.; Wang, L.; Derry, P. J.; Liopo, A.; Zubarev, E. R.; Landes, C. F.; Link, S. Adsorption and Unfolding of a Single Protein Triggers Nanoparticle Aggregation. *ACS Nano* **2016**, *10*, 2103−2112.

(2) Cang, H.; Labno, A.; Lu, C.; Yin, X.; Liu, M.; Gladden, C.; Liu, Y.; Zhang, X. Probing the Electromagnetic Field of a 15-nanometre Hotspot by Single Molecule Imaging. *Nature* **2011**, *469*, 385−388.

(3) Andoy, N. M.; Zhou, X.; Choudhary, E.; Shen, H.; Liu, G.; Chen, P. Single-Molecule Catalysis Mapping Quantifies Site-Specific Activity and Uncovers Radial Activity Gradient on Single 2D Nanocrystals. *J. Am. Chem. Soc.* **2013**, *135*, 1845−1852.

(4) Zhou, X.; Andoy, N. M.; Liu, G.; Choudhary, E.; Han, K.; Shen, H.; Chen, P. Quantitative Super-resolution Imaging Uncovers Reactivity Patterns on Single Nanocatalysts. *Nat. Nanotechnol.* **2012**, *7*, 237−241.

(5) Blythe, K. L.; Mayer, K. M.; Weber, M. L.; Willets, K. A. Ground State Depletion Microscopy for Imaging Interactions between Gold Nanowires and Fluorophore-labeled Ligands. *Phys. Chem. Chem. Phys.* **2013**, *15*, 4136−4145.

(6) Lin, H.; Centeno, S. P.; Su, L.; Kenens, B.; Rocha, S.; Sliwa, M.; Hofkens, J.; Uji-i, H. Mapping of Surface-Enhanced Fluorescence on Metal Nanoparticles using Super-Resolution Photoactivation Localization Microscopy. *ChemPhysChem* **2012**, *13*, 973−981.

(7) Steuwe, C.; Erdelyi, M.; Szekeres, G.; Csete, M.; Baumberg, J. J.; Mahajan, S.; Kaminski, C. F. Visualizing Electromagnetic Fields at the Nanoscale by Single Molecule Localization. *Nano Lett.* **2015**, *15*, 3217−3223.

(8) Blythe, K. L.; Titus, E. J.; Willets, K. A. Triplet-State-Mediated Super-Resolution Imaging of Fluorophore-Labeled Gold Nanorods. *ChemPhysChem* **2014**, *15*, 784−793.

(9) Simoncelli, S.; Roberti, M. J.; Araoz, B.; Bossi, M. L.; Aramendia, P. F. Mapping the Fluorescence Performance of a Photochromic-Fluorescent System Coupled with Gold Nanoparticles at the Single-Molecule-Single-Particle Level. *J. Am. Chem. Soc.* **2014**, *136*, 6878−6880.

(10) Wertz, E.; Isaacoff, B. P.; Flynn, J. D.; Biteen, J. S. Single-Molecule Super-Resolution Microscopy Reveals How Light Couples to a Plasmonic Nanoantenna on the Nanometer Scale. *Nano Lett.* **2015**, *15*, 2662−2670.

(11) Flynn, J. D.; Haas, B. L.; Biteen, J. S. Plasmon-Enhanced Fluorescence from Single Proteins in Living Bacteria. *J. Phys. Chem. C* **2016**, *120*, 20512−20517.

(12) Blythe, K. L.; Titus, E. J.; Willets, K. A. Comparing the Accuracy of Reconstructed Image Size in Super-Resolution Imaging of Fluorophore-Labeled Gold Nanorods Using Different Fit Models. *J. Phys. Chem. C* **2015**, *119*, 19333−19343.

(13) Su, L.; Lu, G.; Kenens, B.; Rocha, S.; Fron, E.; Yuan, H.; Chen, C.; Van Dorpe, P.; Roeffaers, M. B. J.; Mizuno, H.; Hofkens, J.; Hutchison, J. A.; Uji-i, H. Visualization of Molecular Fluorescence Point Spread Functions via Remote Excitation Switching Fluorescence Microscopy. *Nat. Commun.* **2015**, *6*, 6287−6295.

(14) Titus, E. J.; Willets, K. A. Accuracy of Superlocalization Imaging Using Gaussian and Dipole Emission Point-Spread Functions for Modeling Gold Nanorod Luminescence. *ACS Nano* **2013**, *7*, 6258−6267.

(15) Fu, B.; Flynn, J. D.; Isaacoff, B. P.; Rowland, D. J.; Biteen, J. S. Super-Resolving the Distance-Dependent Plasmon-Enhanced Fluorescence of Single Dye and Fluorescent Protein Molecules. *J. Phys. Chem. C* **2015**, *119*, 19350−19358.

(16) Taminiau, T. H.; Stefani, F. D.; Segerink, F. B.; van Hulst, N. F. Optical Antennas Direct Single-Molecule Emission. *Nat. Photonics* **2008**, *2*, 234−237.

(17) Calander, N.; Willander, M. Theory of Surface-plasmon Resonance Optical-field Enhancement at Prolate Spheroids. *J. Appl. Phys.* **2002**, *92*, 4878−4884.

(18) Maier, S. A.; Atwater, H. A. Plasmonics: Localization and Guiding of Electromagnetic Energy in Metal/Dielectric Structures. *J. Appl. Phys.* **2005**, *98*, 011101.

(19) Kinkhabwala, A.; Yu, Z.; Fan, S.; Avlasevich, Y.; Mullen, K.; Moerner, W. E. Large Single-Molecule Fluorescence Enhancements Produced by a Bowtie Nanoantenna. *Nat. Photonics* **2009**, *3*, 654−657.

(20) Tam, F.; Goodrich, G. P.; Johnson, B. R.; Halas, N. J. Plasmonic Enhancement of Molecular Fluorescence. *Nano Lett.* **2007**, *7*, 496−501.

(21) Anger, P.; Bharadwaj, P.; Novotny, L. Enhancement and Quenching of Single-Molecule Fluorescence. *Phys. Rev. Lett.* **2006**, *96*, 113002.

(22) Thompson, R. E.; Larson, D. R.; Webb, W. W. Precise Nanometer Localization Analysis for Individual Fluorescent Probes. *Biophys. J.* **2002**, *82*, 2775−2783.

(23) Su, L.; Yuan, H.; Lu, G.; Rocha, S.; Orrit, M.; Hofkens, J.; Uji-i, H. Super-Resolution Localization and Defocused Fluorescence Microscopy on Resonantly Coupled Single-Molecule, Single-Nanorod Hybrids. *ACS Nano* **2016**, *10*, 2455−2466.

(24) Lakowicz, J. R.; Chowdury, M. H.; Ray, K.; Zhang, J.; Fu, Y.; Badugu, R.; Sabanayagam, C. R.; Nowaczyk, K.; Szmacinski, H.; Aslan, K.; Geddes, C. D. Plasmon-controlled Fluorescence: A New Detection Technology. *Proc. SPIE* **2006**, *6099*, 609909.

(25) Lakowicz, J. R.; Ray, K.; Chowdhury, M.; Szmacinski, H.; Fu, Y.; Zhang, J.; Nowaczyk, K. Plasmon-controlled Fluorescence: a New Paradigm in Fluorescence Spectroscopy. *Analyst* **2008**, *133*, 1308−1346.

(26) Ming, T.; Chen, H.; Jiang, R.; Li, Q.; Wang, J. Plasmon-Controlled Fluorescence: Beyond the Intensity Enhancement. *J. Phys. Chem. Lett.* **2012**, *3*, 191−202.

(27) Chance, R. R.; Prock, A.; Silbey, R. Frequency Shifts of an Electric-Dipole Transition Near a Partially Reflecting Surface. *Phys. Rev. A: At., Mol., Opt. Phys.* **1975**, *12*, 1448−1452.

(28) Blythe, K. L.; Titus, E. J.; Willets, K. A. Effects of Tuning Fluorophore Density, Identity, and Spacing on Reconstructed Images

DOI: 10.1021/acs.jpclett.6b02569
J. Phys. Chem. Lett. 2017, 8, 299−306

in Super-Resolution Imaging of Fluorophore-Labeled Gold Nanorods. *J. Phys. Chem. C* **2015**, *119*, 28099−28110.
(29) Blythe, K. L.; Willets, K. A. Super-Resolution Imaging of Fluorophore-Labeled DNA Bound to Gold Nanoparticles: A Single-Molecule, Single-Particle Approach. *J. Phys. Chem. C* **2016**, *120*, 803−815.
(30) Chen, J.; Bremauntz, A.; Kisley, L.; Shuang, B.; Landes, C. F. Super-Resolution mbPAINT for Optical Localization of Single-Stranded DNA. *ACS Appl. Mater. Interfaces* **2013**, *5*, 9338−9343.
(31) Schmitt, J.; Decher, G.; Dressick, W. J.; Brandow, S. L.; Geer, R. E.; Shashidhar, R.; Calvert, J. M. Metal Nanoparticle/Polymer Superlattice Films: Fabrication and Control of Layer Structure. *Adv. Mater.* **1997**, *9*, 61−65.
(32) Gole, A.; Murphy, C. J. Polyelectrolyte-Coated Gold Nanorods: Synthesis, Characterization and Immobilization. *Chem. Mater.* **2005**, *17*, 1325−1330.
(33) Ni, W.; Yang, Z.; Chen, H.; Li, L.; Wang, J. Coupling between Molecular and Plasmonic Resonances in Freestanding Dye-Gold Nanorod Hybrid Nanostructures. *J. Am. Chem. Soc.* **2008**, *130*, 6692−6693.
(34) Gong, X.; Gao, C. Influence of Salt on Assembly and Compression of PDADMAC/PSSMA Polyelectrolyte Multilayers. *Phys. Chem. Chem. Phys.* **2009**, *11*, 11577−11586.
(35) Habicht, J.; Schmidt, M.; Rühe, J.; Johannsmann, D. Swelling of Thick Polymer Brushes Investigated with Ellipsometry. *Langmuir* **1999**, *15*, 2460−2465.
(36) Toomey, R.; Freidank, D.; Rühe, J. Swelling Behavior of Thin, Surface-Attached Polymer Networks. *Macromolecules* **2004**, *37*, 882−887.
(37) Higuchi, T.; Konyuba, Y.; Nishiyama, H.; Suga, M.; Takahara, A.; Jinnai, H. Direct Observation of Polyelectrolyte Brushes under Wet and Dry Conditions by Atmospheric Scanning Electron Microscopy. *Microscopy* **2016**, *65*, 139−144.
(38) Shuang, B.; Chen, J.; Kisley, L.; Landes, C. F. Troika of Single Particle Tracking Programing: SNR Enhancement, Particle Identification, and Mapping. *Phys. Chem. Chem. Phys.* **2014**, *16*, 624−634.
(39) Parthasarathy, R. Rapid, Accurate Particle Tracking by Calculation of Radial Symmetry Centers. *Nat. Methods* **2012**, *9*, 724−726.
(40) Sönnichsen, C.; Franzl, T.; Wilk, T.; von Plessen, G.; Feldmann, J.; Wilson, O.; Mulvaney, P. Drastic Reduction of Plasmon Damping in Gold Nanorods. *Phys. Rev. Lett.* **2002**, *88*, 077402.
(41) Kuehn, S.; Hakanson, U.; Rogobete, L.; Sandoghdar, V. Enhancement of Single-Molecule Fluorescence Using a Gold Nanoparticle as an Optical Nanoantenna. *Phys. Rev. Lett.* **2006**, *97*, 017402.
(42) Yuan, H.; Khatua, S.; Zijlstra, P.; Yorulmaz, M.; Orrit, M. Thousand-fold Enhancement of Single-Molecule Fluorescence Near a Single Gold Nanorod. *Angew. Chem., Int. Ed.* **2013**, *52*, 1217−1221.
(43) Reineck, P.; Gomez, D.; Ng, S. H.; Karg, M.; Bell, T.; Mulvaney, P.; Bach, U. Distance and Wavelength Dependent Quenching of Molecular Fluorescence by Au@SiO2 Core-Shell Nanoparticles. *ACS Nano* **2013**, *7*, 6636−6648.
(44) Abadeer, N. S.; Brennan, M. R.; Wilson, W. L.; Murphy, C. J. Distance and Plasmon Wavelength Dependent Fluorescence of Molecules Bound to Silica-Coated Gold Nanorods. *ACS Nano* **2014**, *8*, 8392−8406.
(45) Lin, H.; Chen, I. Study of the Interaction between Gold Nanoparticles and Rose Bengal Fluorophores with Silica Spacers by Time-Resolved Fluorescence Spectroscopy. *J. Phys. Chem. C* **2015**, *119*, 26663−26671.
(46) Goizueta, G.; Chiba, T.; Inoue, T. Phase Morphology of Polymer Blends: 2. SEM Observation by Secondary and Backscattered Electrons from Microtomed and Stained Surface. *Polymer* **1993**, *34*, 253−256.

DOI: 10.1021/acs.jpclett.6b02569
J. Phys. Chem. Lett. 2017, 8, 299−306